Brain Struct Funct (2011) 216:1–15
DOI 10.1007/s00429-010-0291-8

ORIGINAL ARTICLE

Axonal morphometry of hippocampal pyramidal neurons semi-automatically reconstructed after in vivo labeling in different CA3 locations

Deepak Ropireddy · Ruggero Scorcioni · Bonnie Lasher · Gyorgy Buzsáki · Giorgio A. Ascoli

Received: 14 August 2010 / Accepted: 10 November 2010 / Published online: 3 December 2010

Abstract Axonal arbors of principal neurons form the backbone of neuronal networks in the mammalian cortex. Three-dimensional reconstructions of complete axonal trees are invaluable for quantitative analysis and modeling. However, digital data are still sparse due to labor intensity of reconstructing these complex structures. We augmented conventional tracing techniques with computational approaches to reconstruct fully labeled axonal morphologies. We digitized the axons of three rat hippocampal pyramidal cells intracellularly filled in vivo from different CA3 sub-regions: two from areas CA3b and CA3c, respectively, toward the septal pole, and one from the posterior/ventral area (CA3pv) near the temporal pole. The reconstruction system was validated by comparing the morphology of the CA3c neuron with that traced from the same cell by a different operator on a standard commercial setup. Morphometric analysis revealed substantial differences among neurons. Total length ranged from 200 (CA3b) to 500 mm (CA3c), and axonal branching complexity peaked between 1 (CA3b and CA3pv) and 2 mm (CA3c) of Euclidean distance from the soma. Length distribution was analyzed among sub-regions (CA3a,b,c and CA1a,b,c), cytoarchitectonic layers, and longitudinal extent within a three-dimensional template of the rat hippocampus. The CA3b axon extended thrice more collaterals within CA3 than into CA1. On the contrary, the CA3c projection was double into CA1 than within CA3. Moreover, the CA3b axon extension was equal between strata oriens and radiatum, while the CA3c axon displayed an oriens/radiatum ratio of 1:6. The axonal distribution of the CA3pv neuron was intermediate between those of the CA3b and CA3c neurons both relative to sub-regions and layers, with uniform collateral presence across CA3/CA1 and moderate preponderance of radiatum over oriens. In contrast with the dramatic sub-region and layer differences, the axon longitudinal spread around the soma was similar for the three neurons. To fully characterize the axonal diversity of CA3 principal neurons will require higher-throughput reconstruction systems beyond the threefold speed-up of the method adopted here.

Keywords Axonal arbors · CA3c · CA3b · Digital morphology · Hippocampus · Principal neuron · Schaffer collateral

D. Ropireddy · R. Scorcioni · B. Lasher · G. A. Ascoli (✉)
Center for Neural Informatics, Structures, and Plasticity, Molecular Neuroscience Department, Krasnow Institute for Advanced Study, George Mason University, MS#2A1, 4400 University Drive, Fairfax, VA 22030, USA
e-mail: ascoli@gmu.edu

Present Address:
R. Scorcioni
The Neurosciences Institute, La Jolla, CA, USA

Present Address:
B. Lasher
Baylor University, Waco, TX, USA

G. Buzsáki
Center for Molecular and Behavioral Neuroscience, Rutgers University, Newark, NJ, USA

Introduction

The pioneering work of Ramón y Cajal more than a century ago revealed the intricate structure of dendritic and axonal processes in the central nervous system (Ramón y Cajal 1911). Since then, a great deal of information has been gathered about the complex three-dimensional morphology

of principal neurons in the mammalian hippocampus (e.g. Ishizuka et al. 1995; Turner et al. 1995; Pyapali et al. 1998). In particular, axonal arbors of pyramidal cells in area CA3 are much more extensive than their dendritic counterparts, reaching out to hundreds of thousands of potential post-synaptic targets (Ishizuka et al. 1990; Li et al. 1994; Wittner et al. 2007). The CA3 region emanates the richest network of axonal projections in the rodent hippocampus, with collaterals and commissurals projecting bilaterally to both CA3 and CA1 principal cells as well as interneurons (Li et al. 1994; Witter and Amaral 2004).

On the one hand, the dense and far-reaching arborization of CA3 pyramidal cell axons provides the backbone for the circuitry underlying autoassociative computation, a putatively fundamental function of the hippocampus (Rolls 2007). The importance of region CA3 in the hippocampus is well documented from memory encoding and retrieval (Treves and Rolls 1994; Treves 2004; Kunec et al. 2005) through generation of hippocampal rhythms (Buzsaki 1986; Csicsvari et al. 2003). The structure and connectivity of CA3 pyramidal neurons vary substantially with their transverse and longitudinal locations (Witter 2007). Thus, a comprehensive understanding of the dynamic mechanisms of hippocampal learning will likely require a quantitative map of the entire axonal arbors originating from different network sub-regions.

On the other hand, this same structural complexity renders the 3D digital reconstruction of these axons exceedingly labor-intensive, time-consuming, and error-prone with conventional methods (such as Microbrightfield Neurolucida). Only one complete axon has been digitally reconstructed from CA3 pyramidal cells (Wittner et al. 2007), while other reports were based on serial two-dimensional tracings that, while more practical, only allow limited analysis (Sik et al. 1993; Li et al. 1994). More generally, among the morphological reconstructions publicly available at NeuroMorpho.Org (Ascoli et al. 2007), the proportion of dendrites far outweighs that of axons (even if incomplete). To alleviate this problem, we recently devised a reconstruction technique combining 2D tracing with an algorithmic approach. Similar hybrid methodologies had been only previously applied to dendritic trees (Wolf et al. 1995). We employed our original design (Scorcioni and Ascoli 2005) to reconstruct entire 3D axonal arbors from two-dimensional tablet tracings of several principal neurons from various regions of the hippocampal complex (e.g. Tamamaki et al. 1988; Tamamaki and Nojyo 1995).

Here, we further developed our method to extend its applicability to the more general Camera Lucida (pencil-on-paper) tracings. Such refinement enables the digital retrieval of full 3D reconstructions of neuronal arbors manually traced from serial section staining. Using this technique, we reconstructed the axonal arbors of hippocampal pyramidal cells intracellularly labeled in vivo from three sub-regions of area CA3 (Li et al. 1994). Two neurons were from areas CA3b and CA3c, respectively, of the dorsal hippocampus (towards the septal pole). The third neuron was from the posterior/ventral area (CA3pv) in the temporal pole. The reconstruction system was validated by comparing the morphology of the CA3c neuron with that traced from the same cell by a different operator on a standard commercial setup (Wittner et al. 2007).

In addition to quantifying the intrinsic morphology of these axons, we evaluated their spatial extension within various hippocampal regions and layers by digitally embedding the arbors within a 3D template of the rat hippocampus based on high-resolution imaging of thin histological sections (Ropireddy et al. 2008). This analysis reveals similarities between the two reconstructions of the same CA3c cell, and dramatic differences from the other two neurons (CA3b and CA3pv). We discuss the implications of these findings for systems level connectivity and the potential functional consequences for existing theories of hippocampal cognitive processing.

Materials and methods

In the present work, a new axonal reconstruction pipeline is developed for and applied to Sprague-Dawley rat CA3 pyramidal neurons intracellularly filled in vivo with biocytin (Li et al. 1994; Wittner et al. 2007). The experimental details of the histological preparation are described in those previous reports and are only summarized here. Briefly, neurons were located stereotactically and identified electrophysiologically, and animals were perfused 2 h after injection. After brain removal and fixation, 70 μm coronal sections were incubated in avidin–biotin horseradish peroxidase (HRP) complex and stained by 3,3′-diaminobenzidine-4HCl (DAB) intensified with $Ni(NH_4)SO_4$. Slices were mounted on gelatin-coated slides and covered with DePeX. The reconstruction and analysis procedures described below extend our previous development (Scorcioni and Ascoli 2005) and are expected to be also suitable for rapid Golgi preparations.

Nomenclature

In this study, we follow the hippocampal anatomical terminology originally introduced by Lorente de Nó (1934) and subsequently adopted in numerous reports (e.g. Ishizuka et al. 1990, 1995; Li et al. 1994; Witter and Amaral 2004). The long axis of the hippocampus curves from the septal pole located dorsally in the most anterior end, to the temporal pole, located ventrally after passing the most posterior end. Transverse to this longitudinal

curvature, Cornu Ammonis (CA) is divided into seven adjacent sub-regions, namely CA1a, CA1b, CA1c, CA2, CA3a, CA3b, and CA3c. CA1a lies near the subiculum, while CA3c is located between the supra- and infra-pyramidal blades of the dentate gyrus (Fig. 1a). CA3a is the region of maximum curvature at the origin of the fornix, while CA1b may be recognized as the straightest CA1 sub-region. Because of its small size, CA2 is not always identifiable in all slices, and here we consider it lumped together with CA3a. Along the depth of the transverse plane, four cytoarchitectonic layers are identifiable throughout CA, named (from outermost to innermost) stratum oriens (bordering the alveus), stratum pyramidale, stratum radiatum, and stratum lacunosum-moleculare (bordering the fissure). Since stratum lucidum, the mossy fiber layer, is present in CA3 but not CA1, here we consider it lumped together with stratum radiatum.

In this work, three CA3 pyramidal cells are characterized. The somata of two of them are located in the dorsal hippocampus, in sub-regions CA3c and CA3b, respectively. The soma of the third neuron is in the posterior/ventral (CA3pv) region. For the sake of interpretability, we refer to these cells in the text by the names of these sub-regions, but this notation should not be confused to indicate the axonal distribution of these cells, which is spread across all sub-regions. In order to maximize clarity of cross-referencing, here and throughout the captions within the figures we report the correspondence between these cells and their original identifiers used in previous papers. In particular, our reconstructions of neurons CA3b and CA3pv correspond to cells 51 and 60a, respectively (Turner et al. 1995). Our reconstructions of neuron CA3c correspond to cell D256 (Wittner et al. 2007). This CA3c cell was also previously traced with the standard commercial system Microbrightfield NeuroLucida. This earlier digital reconstruction is referred here by the use of the superscript NL ($CA3c^{NL}$) to distinguish it from the morphology reconstructed with the system described below.

Slide inspection, sequential alignment, and tracing

Microscope slides are initially evaluated in order to identify and number the tissue slices containing portions of the stained neuron arbors (Fig. 1a). The amount of rotational difference between adjacent slices is calculated based on matching blood vessels and other landmarks so as to allow later alignment of traced neuronal data. Tracing is performed on an Olympus BX51 microscope equipped with Camera Lucida and an achromatic 40× dry objective with numerical aperture of 0.65. All visible dendritic and axonal

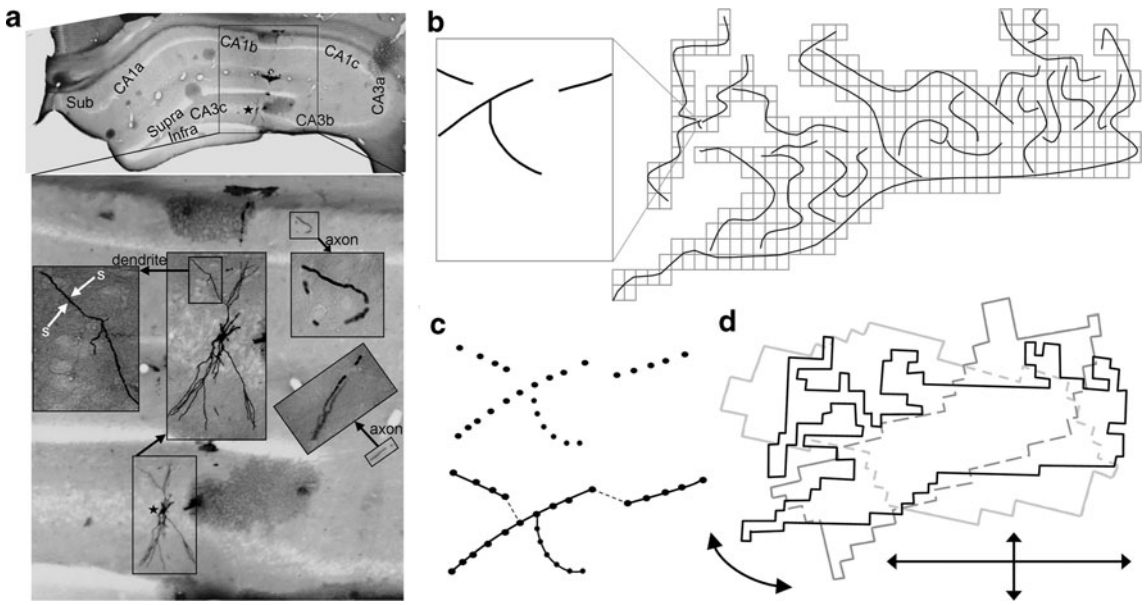

Fig. 1 Axonal reconstruction process: from micrographs to digital trees. **a** Representative micrographs of dorsal hippocampus captured by lenses with different magnification power: ×4 (*top*) with captioned sub-regions (*Sub*, *Supra*, and *Infra* indicate subiculum and the two granular blades of the dentate gyrus, respectively) and *asterisk* marking the somatic position within CA3c; ×8 (*bottom*) with visible dendritic tree further enlarged at ×20 and ×40 (*boxed insets* indicated by *black arrows*) to highlight branches and spines (*white* '*s*' *arrows*), as well as two axonal stretches enlarged at ×40. **b** Illustration of a single labeled slice tracing, assembled from dozens of US letter-sized sheets of paper tiled together, each with manually pencil-traced neurites. One sheet is enlarged on the left, showing representative line traces. **c** After high-resolution serial scanning, tracing images (here represented for one sheet only) are digitized into pixel format and vectorized. *Dashed lines* represent untraced segments joined by nearest-neighborhood. **d** In the 3D arbor-stitching step, all planar vector sets, each corresponding to a histological section, are first aligned by translation and rotation. Then, they are joined together in 3D using information of the apparent terminations marked to be in focus at the *top* or *bottom* of the slice

segments through the slice depth are manually traced on regular paper pre-printed with a black box demarking 1 inch margins. The fields of view within these boxes represent unitary regions of interest (Fig. 1b) whose relative spatial position is labeled on the sheet with a univocal alphanumeric designation. For example, the adjacent boxes on the top, right, bottom, and left of the box in sheet M3 are found on sheets L3, M4, N3, and M2, respectively. Neurites and landmarks falling within an inch from the box borders are re-traced outside of the box borders of the appropriate adjacent sheets. These duplicate tracings allow later alignment of corresponding fields of views.

Distinguishing between bifurcation points and axonal crossings constitutes one of the toughest challenges in automated tracing (see, e.g., http://diademchallenge.org). In most cases, however, this determination is relatively easy for the human eye. In the reconstructions described here, such distinction always occurs at the time of pencil-on-paper tracing, and not as an unsupervised algorithmic step. Moreover, multiple colors are used to indicate variable thickness estimates: axons are assigned approximate diameters of 1, 0.5, and 0.1 μm, and dendrites of 3 and 0.3 μm, respectively. When axons and dendrites are both present in the same field of view, they are drawn on separate sheets of paper with identical alphanumerical identity. This produces a separate reconstruction of dendrites that is later merged to the axonal reconstruction during the digital reconstruction process (described below). The choice to only discriminate among a limited set of neurite thickness values was the fruit of a compromise between manual labor and retained biological information. Soma and landmarks were also distinctly color-coded. Subsequent image processing was found to be sensitive to ink quality, and produced optimal results with Pigma Micron (http://sakuraofamerica.com/Pen-Archival).

Apparent neurite terminations observed within the top and bottom 10% of the slice depth, assumed to constitute slicing truncations, are marked with small (~2 mm diameter) and large (~5 mm diameter) pink circles, respectively. These circle tracings are utilized in the digital reconstruction process (described below) in order to both identify inter-slice continuations and assign their Z coordinate. In the absence of a circle, neurite tips are treated as real terminations. The axons reconstructed in the present work traversed between 50 and 60 tissue slices. Every slice required up to 75 sheets to trace. Each neuron required approximately 3 weeks of full-time work to trace.

Image acquisition and pre-processing

Tracing papers are digitized with a MicroTeK ScanMaker 5950 automated scanner (http://microtek.com), with 1,200 dpi resolution and a color depth of 24 bits. Up to 30 sheets of paper are fed to the machine at a time. To minimize deformation due to lamp warm-up, a batch of 30 scans are rescanned if the scanner was not in use for more than 2 h. The resulting digital picture is manually renamed with the sheet alphanumerical designation within that particular slice (for example, if the paper sheet is labeled N20, its output scan is saved as N20.jpg). All images belonging to a particular slice are stored in a directory whose name reflects the slice number itself.

The color intensity of the scanner output must be digitally equalized to control for the effects of ambient temperature, vibration, light bulb lifetime, and use hours. During equalization all papers are digitally processed to identify the average white background level (by averaging all pixels in the picture) and the darkest black present (by selecting the pixel with the lowest intensity). Once these two values are identified, all colors are equalized between these two extremes. All digitized tracings are processed on a Windows-based PC (dual Xeon 3 GHz, 2 GB RAM, 120 GB disk) with a set of ad-hoc Java and Perl scripts. At this stage, the optimal translation offset is also manually estimated between all pairs of adjacent images based on corresponding landmarks and on the overlap of the neurites double-traced outside of the black box boundaries.

All scanned papers are processed to crop the margins outside of the boxed area. While reducing acquisition time, automated scanning introduces two types of distortions in the final scanned image: mechanical deformations and color quality reproduction. The latter is particularly apparent by the non-uniform range of gray shades corresponding to the pixels of black frame. Both of these issues render the cropping phase problematic and are solved with an additional post-processing step, also implemented in Java. In particular, the most likely box position is identified with a pixel-by-pixel search algorithm based on color intensity and an extended spatial range of 10 pixels from the maximum values. To simplify the correct color identification of dendritic and axonal thickness in the subsequent reconstruction, landmarks are also removed at this point. This step uses the Adobe Photoshop color removal tool with a similarity threshold of 60% to recursively identify and erase all relevant shades of pink. After human-validation for quality, all cropped images are algorithmically tiled into a digital canvas based on their alphanumerical identifiers and the pair-wise offset information obtained from the duplicate tracing overlaps (Fig. 1b).

Digital reconstruction of arbor morphology

The algorithmic reconstruction of the scanned images into digital arbors requires converting raster images (pixel coordinates) to vectors (segments). This step is performed

on each of the 2D digital canvases individually with the freeware version of the Wintopo commercial package (Softsoft.net, Bedfordshire, UK). In particular, optimal vector extraction is obtained by selecting the "Stentiford thinning" method and setting the tolerance of the "Smooth Polyline Vectorization" to 30 (the units of this parameter are tenths of pixel widths, so this setting corresponds to 3 pixels). The value of the option "Reduce Polylines During Vectorization" is also set to 30. Wintopo output is saved in ASCII format (Fig. 1c).

The *Z* coordinate of each point is first determined on the basis of the sequential order of the specific section. Points that lie either at the top or bottom of the slice are identified, respectively, by small and large circles as described earlier. Circles are algorithmically recognized as poly-lines with starting and ending points characterized by the same 2D coordinates. The circle position and radius are then computed as the mean and standard deviation of the *X* and *Y* coordinates of all the points belonging to the poly-line. The *Z* coordinate of the neurite closest to the circle position is then corrected by ±33% of the inter-slice distance depending on the circle diameter. Sequential digital canvases in the *Z* stack were manually aligned by translation and rotation (Fig. 1d).

Next, diameter values are added to the 3D vector data based on color. Each individual point color is assigned to its corresponding diameter and neurite type, as described earlier. Unfortunately, however, color varies by the specific batch of paper, as well as by the angle, speed, and pressure of the pen used for the tracing. Since these properties can only be controlled in a limited way, custom software is used for color identification. A sample of each color pen trait is first scanned and assigned to its color, averaged across all its neighborhood pixels that are not part of the background (typically ~10 pixels). This average is compared with the mean color components, and the component closest to the measured value is assigned to the pixel.

Finally, 3D arbors are connected with the algorithm previously developed to reconstruct axonal trees from tablet data (Scorcioni and Ascoli 2005). Since this procedure was described previously in detail, and employed without modification, it is only summarized here. All vector data with their assigned type are loaded into memory. Each point is then compared with all other points that do not belong to the same line. At each step the set of points that is closest to each other are joined in the same line. This process is repeated until only one line is left. The soma position, identified by its color type, is selected as the starting point. The structure is then recursively parsed to create the corresponding digital output in SWC format (Ascoli et al. 2007).

Conversions among unit distances in the slice, tracing paper, scanned images, and digital reconstructions were calculated by first tracing the grid from a micron-scale calibration slide. The resulting length was then measured on the sheet with a standard ruler. Next, the number of pixels in the unit lines was counted on the corresponding image. Finally, the resulting numerical coordinates in the vectorized digital reconstruction were converted back to the original micron values. In particular, 1 cm on paper corresponded to 12.3 μm on the slide and in the digital reconstruction file, and to 78.35 image pixels (200 dots-per-inch or dpi), corresponding to 6.37 pixels/μm.

Hippocampus 3D embedding and morphometric analysis

In order to evaluate the morphological organization of the axonal arbors within the hippocampal cytoarchitecture, we embedded the digital reconstructions into a 3D template of the rat hippocampus previously created from thin histological sections. The details of this 3D template were extensively described (Ropireddy et al. 2008) and are thus only briefly reported here. Serial coronal images were obtained with an EPSON 3200 dpi scanner from Nissl-stained 16 μm cryostatic slices. Four cytoarchitectonic layers of Cornu Ammonis were segmented in each image, namely strata oriens, pyramidale, radiatum, and lacunosum-moleculare. The images and 2D segmentations were sequentially registered over the whole rostro-caudal extent. Digitized 3D volumes were extracted with a voxelizing algorithm (custom-developed in C/C++) at 16 μm isotropic resolution. Each voxel in the template is tagged with two sets of coordinates. The first set corresponds to the main hippocampal axes: longitudinal, along the septo-temporal curvature; transversal, along the DG and CA "C"-like shapes; and depth, perpendicular to the first two. The second set of coordinates follows the canonical brain orientations, namely rostro-caudal, medio-lateral, and dorso-ventral. Moreover, voxels are also marked in the template with their sub-region and layer identity (e.g. CA3c stratum oriens, DG supra-pyramidal blade stratum moleculare, etc.).

After the voxelization step, the digitally reconstructed neuronal arbors are embedded within the 3D volume of the hippocampus such as to map their somatic position to the location reported for the intracellular electrode (Li et al. 1994; Turner et al. 1995 and Wittner et al. 2007). In particular, the CA3b (cell 51 in Li et al. 1994) and CA3pv (cell 60 in Li et al. 1994, also called 60a in Turner et al. 1995) neurons had the same pair of stereotactic coordinates AP = 2.4 mm and ML = 2.5 mm from bregma. These original papers also describe the locations of the first two neurons as septal/dorsal (CA3b cell) and posterior/ventral (CA3pv cell), which allows the unique identification of the depth position corresponding to the pyramidal layer

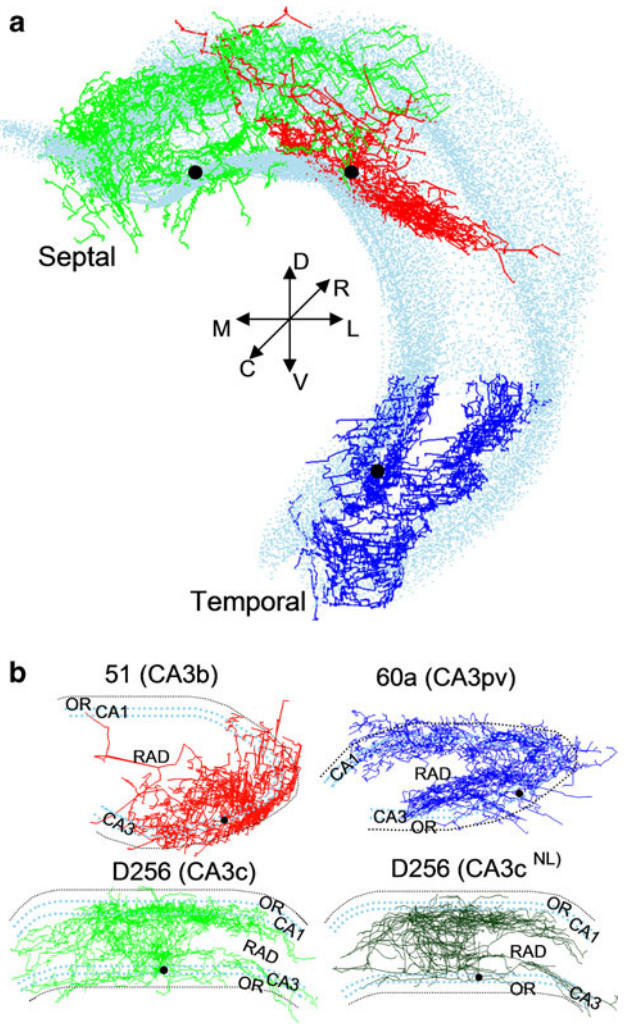

Fig. 2 Digital rendering of reconstructed CA3 pyramidal cell axons. **a** Axonal arbors of neurons with somatic locations (*black dots*) in different CA3 sub-regions (CA3b *red*; CA3pv *blue*; and CA3c *green*) 3D-embedded within the rat hippocampal template, with *arrow captions* indicating dorso-ventral (D/V), medio-lateral (M/L) and rostro-caudal (R/C) orientations. **b** Individual renderings of the four CA3 axonal reconstructions (including $CA3c^{NL}$), with fiduciary boundaries showing strata oriens (OR) and radiatum (RAD) and the pyramidal layer marked in *light blue color*

(Fig. 2a). The CA3c neuron (cell D256, Wittner et al. 2007) had stereotactic coordinates AP = 3.5 mm and ML = 2.5 mm from bregma. The somatic location in the 3D template was determined for each neuron as the center of the sets of voxels within stratum pyramidale corresponding to the reported stereotactic coordinates. The digital arbors are initially oriented so that their primary dendritic axis is perpendicular to the longitudinal curvature of the principal layer, and their secondary dendritic axis is parallel to the transverse plane (Ropireddy et al. 2008). This initial orientation is then manually fine-tuned so as to maximize the portion of the axonal tree contained within the volume boundaries of the hippocampus. This additional step of manual optimization was limited in all cases to an angular value of ±30°.

Intrinsic morphometric parameters, such as axonal path length and bifurcation numbers, are extracted using L-Measure (http://krasnow.gmu.edu/cn3), a freeware tool for morphological analyses of neuronal arbors (Scorcioni et al. 2008). The axonal arbors embedded in the 3D template are amenable to a detailed analysis of the distribution of length along the hippocampal and brain coordinates, and within individual cytoarchitectonic layers and sub-regions. For accomplishing this task, an algorithm is designed to compute the coordinates of intersection between an axonal segment and the boundaries of the voxel. This process enables the measurement of the axonal length enclosed within a voxel. After all voxels are probed, axonal length is summed according to one of the above-described hippocampal or brain coordinates, as well as to specific sub-regions and layers. All graphs are plotted with OriginPro 8.0 software (http://originlab.com) unless otherwise noted.

Results

Practical assessment of the reconstruction technique

The devised semi-automated reconstruction technique combines conventional tracing methodology (pencil-on-paper) with algorithmic processing to digitize the drawn morphology into a vector format (Fig. 1). Intracellularly filled CA3 pyramidal cells display sufficient contrast for reliable tracing at high magnification (Fig. 1a). However, the sheer size of the axonal trees of these neurons and the spatial extent of the tissue region they invade pose a formidable challenge for the complete reconstruction of these arbors. Conventional tracing is much faster and more practical than the direct digital reconstruction of neuronal arbors enabled by modern computer-interfaced microscopes and commercial software (e.g. Microbrightfield NeuroLucida). For example, the CA3c pyramidal cell described both here and previously (Wittner et al. 2007) required more than 6 months of full-time labor to reconstruct the entire axonal arbor with NeuroLucida ($CA3c^{NL}$), compared with only 3 weeks of pencil-on-paper tracing. By itself, however, this process only yields a very large number of letter-sized sheets for each of the serial sections (Fig. 1b), which sums up to several thousand for the whole axonal tree (e.g. ~3,200 for neuron CA3c).

This amount of raw data still constitutes a substantial limiting factor in the implementation of the algorithmic pipeline described in "Materials and methods". The number of peculiarities and exceptions in the data is too large to fully automate every processing step. Therefore,

although the actual computing time is relatively negligible, the sheer execution of the procedure leading from the manual tracings to the digital reconstruction requires almost as much time as the drawing itself. Moreover, the product of this procedure still requires considerable human intervention to ensure rigorous quality control. In particular, partial 2D projections of the digital reconstruction must be checked against the corresponding tiled images. Once again, although this operation is not unique or even uncommon, the exquisite number of sections and size of each makes this necessary step notably time consuming. More specifically, quality checks and related corrections and adjustments cost in our hands approximately the same amount of time as each of the previous two aspects (manual tracing and execution of the algorithm pipeline).

As a result, the full reconstruction of complete CA3 pyramidal cell axons from mounted slides to finalized digital files is estimated to take approximately 9 weeks of full-time skilled labor per neuron with this technique. This is a definitive improvement compared with the 6 months required by existing state-of-the-art solutions, and enabled the first quantitative comparative analysis of three axonal morphologies, which is described below.

3D appearance and intrinsic morphometry of CA3 pyramidal cell axons

The digital reconstructions of the traced neurons were embedded in the hippocampal 3D template (Fig. 2) as described in "Materials and methods". The three somata were located in area CA3c near the septal pole (cell D256 in Wittner et al. 2007), area CA3b towards the middle of the longitudinal axis (cell 51 in Li et al. 1994), and area posterior/ventral or CA3pv near the temporal pole (cell 60 in Figs. 1, 2, and 12 of Li et al. 1994; cell 60a in Turner et al. 1995), respectively (Fig. 2a). Each of the three neurons displayed a uniquely distinct arbor shape. The digital reconstruction previously acquired with the standard NeuroLucida system by a different operator ($CA3c^{NL}$) was recognizably similar to the morphology traced from the same slides with the present system (Fig. 2b). In each of the three neurons, the axonal extent spanned a sizeable proportion of the whole hippocampus (Fig. 2a), far exceeding the reach of the same neuron's dendrites. The ratios between total dendritic and axonal lengths were 1:13 (CA3b), 1:22 (CA3pv), and 1:27 (CA3c). The CA3c neuron had the longest axonal branching (nearly half-a-meter), and this value differed <0.5% from that of $CA3c^{NL}$.

The large axonal extent of CA3 pyramidal neurons prompts the question of how this length is distributed in space. A simple characterization ("Sholl" plot) can be obtained from conventional tracings by drawing several concentric circles around the soma location and plotting the number of branch intersections against the circle radius. Digital reconstructions allow a more direct representation of the axonal amount by providing a path length measure instead of relying on intersections. Moreover, 3D information can be extracted by using Euclidean distance from the soma instead of circular projections. The CA3 pyramidal cell reconstructions were compared with this approach (Fig. 3a). In the face of the large differences in total axonal lengths (the CA3c neuron being twice as long as the CA3b one), the contrast among the reconstructed neurons in other aspects appeared more modest. For example, the maximum Euclidean distance from the soma reached by the axonal trees only varied from above 3 mm for the CA3b neuron to below 4 mm for the CA3c one. Similarly, the "median" distance corresponding to the radius of a sphere

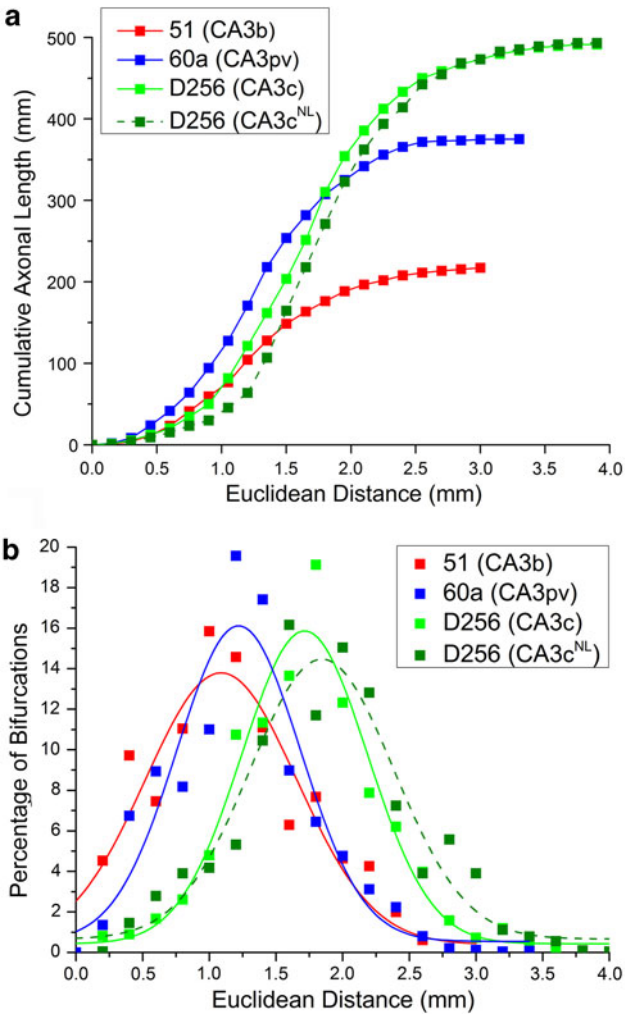

Fig. 3 Intrinsic morphometry of CA3 pyramidal cell axons. **a** Cumulative axonal length as a function of Euclidean distance from the soma for each of the four neurons (CA3b *red*; CA3pv *blue*; CA3c *light green*; and $CA3c^{NL}$ *dark green*). **b** Distribution of the proportion of arbor bifurcations with respect to Euclidean distance from the soma, overlaid with Gaussian curve fits

encompassing 50% of the whole axonal extension was 1.3 and 1.7 mm, respectively, for the same two neurons. Both maximum and median distances, but not total length, were also very similar between the CA3b and CA3pv neurons.

An alternative variation of Sholl plots analyses the proportion of bifurcation points as a function of the 3D distance from the soma (Fig. 3b), providing an indication of tree complexity. These measures fall at similar distances from the soma for the CA3b and CA3pv neurons (1.1 and 1.2 mm, respectively), but farther for the CA3c cell (1.7 mm). The spread of these distributions (computed as standard deviation) is essentially identical for all cells, tightly ranging from 1 to 1.1 mm. Similarly, the peak values of these distributions are also constrained within a narrow span between 13.4% (CA3b), and 15.6% (CA3pv). Moreover, the measures of all of these parameters for the CA3c neuron differ by <5% from the corresponding values of CA3c^{NL}, suggesting that these summary metrics of digital reconstructions of the same neuron are reproducible across tracing techniques and operators.

Distinct 3D axonal projections of CA3 pyramidal cells across the hippocampus

The embedding of the digital reconstruction in the 3D hippocampus template allows the analysis of axonal length within anatomically identifiable dimensions (Fig. 4). We first measured the axonal distributions across the septo-temporal direction, which represents the main longitudinal axis of the hippocampus. The somatic locations of the reconstructed neurons are uniformly distanced along this axis (Fig. 4a). With minimal overlap, the three axonal arbors collectively cover almost the entirety of the longitudinal span. The septo-temporal extent (the "width" of the curves in Fig. 4a) is similar for all neurons, with a half-height span of ~1.5 mm. While the length distribution is approximately symmetric around the soma for neuron CA3c, it is skewed septally in neuron CA3b and temporally in neuron CA3pv. Interestingly, however, the peak of the distribution is septal relative to the soma for all the three neuronal types.

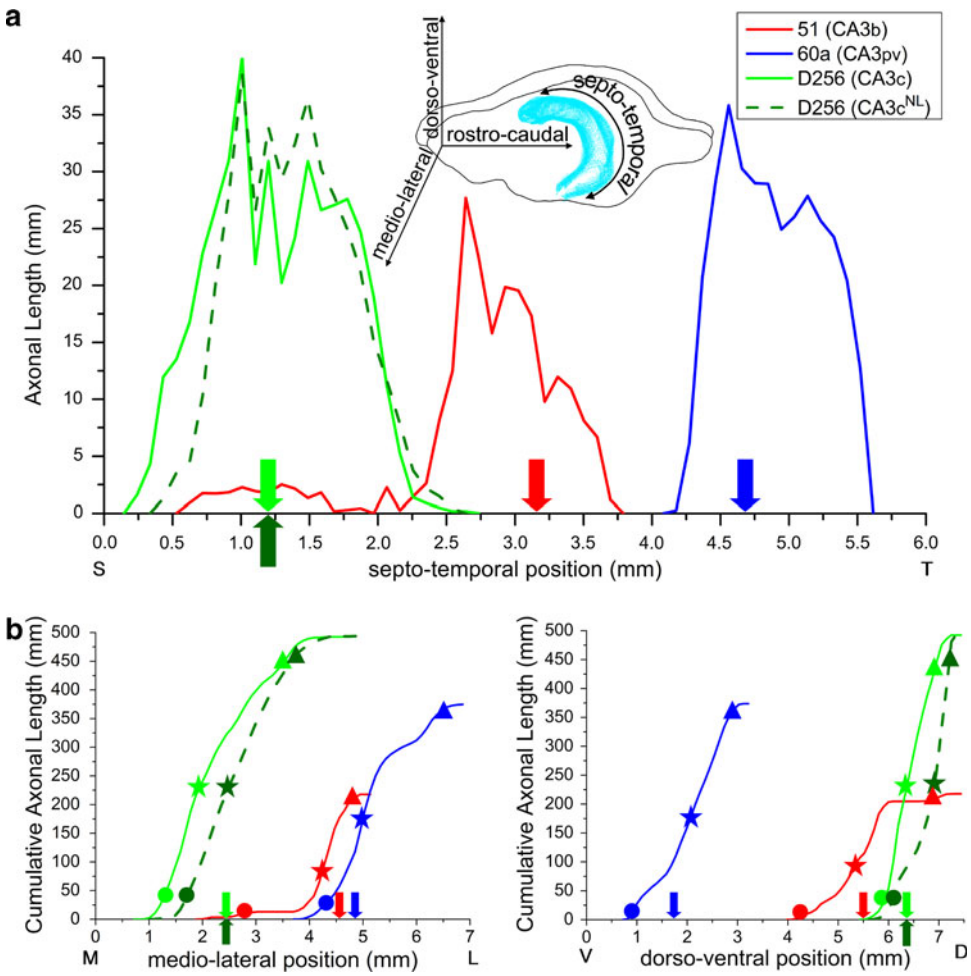

Fig. 4 Axonal length distribution along main hippocampus axes and canonical brain orientations. **a** Differential distribution of axonal projections in the septo-temporal axis for the reconstructed neurons (CA3b *red*; CA3pv *blue*; CA3c *light green*; and CA3c^{NL} *dark green*). The captions 'S' and 'T' on the abscissa indicate septal and temporal directions, respectively and *arrows* point to corresponding soma positions. The *inset* illustrates the position of the hippocampus (*light blue*) within an outline of the rat brain, relating the canonical hippocampus and brain axes. **b** Cumulative axonal length distributions in the medio-lateral (*left panel*) and dorso-ventral (*right panel*) orientations. *Solid circles*, *stars*, and *triangles* represent the 5th, 50th, and 95th percentiles of the axonal length for every neuron. The captions 'M', 'L', 'V', and 'D' on the abscissa indicate medial, lateral, ventral, and dorsal directions, respectively

Next, we examined the axonal projections against the canonical brain axes most univocally relevant to the hippocampal orientation, namely dorso-ventral and medio-lateral, corresponding to horizontal and sagittal planes, respectively (Fig. 4b). In the dorso-ventral direction, the axonal span differs substantially among the CA3 pyramidal cells. This is evident from the position at which each of these axonal arbors crosses the 5th, 50th, and 95th length percentiles (Fig. 4b, left panel). For the CA3c neuron, 90% of the total axonal length falls within less than a millimeter. For the CA3b neuron, the same relative span is nearly three times broader (>2.5 mm). A similar trend is observed in the medio-lateral direction (Fig. 4b, right panel). In all cases, the median position falls close to the soma.

Similar to the intrinsic morphometrics, the two digital morphologies traced from the same neuron by independent operators and with different reconstruction systems (CA3c and CA3c^{NL}) have comparable length distributions relative both to the hippocampus (Fig. 4a) and brain (Fig. 4b) axes.

CA3 pyramidal cell axons differ in their sub-region and layer patterns

A distinguishing aspect of CA3 pyramidal neurons within the hippocampal circuit is that their axons overlap with both basal and apical dendrites of principal cells throughout CA3 (recurrent collaterals) and CA1 (Schaffer collaterals). The digital embedding of axonal reconstructions in a 3D cytoarchitectonic template provides the exquisite opportunity to comparatively quantify among individual morphologies the axonal proportions in different layers and sub-regions throughout their longitudinal extents (Fig. 5). The three reconstructed neurons vary strikingly in the axonal arbor length invading CA3 versus CA1. The definite majority (three fourths) of the axonal arbor from the CA3b cell is confined in CA3. On the contrary, only a minority (two fifth) of the axon of the CA3c neuron remains in CA3. Interestingly, the CA3pv cell presents an intermediate pattern, with a nearly identical split between CA3 and CA1 axonal projections.

These relative fractions are in qualitative agreement with previous observations (Ishizuka et al. 1990; Li et al. 1994), yet they follow non-trivially from the absolute lengths (Fig. 5a). In light of their considerable difference in total extent, the amount of axon cable invading CA3 is remarkably similar among the three neurons (e.g. 160 mm for the CA3b cell vs. 175 mm for the CA3c cell). In contrast, absolute length differences are exacerbated in the projections to CA1, with the CA3c cell (315 mm) overwhelming the CA3b (95 mm) more than threefold.

The axonal patterns of the three CA3 pyramidal cell morphologies are also highly non-uniform across the individual sub-regions of CA3 and CA1. For both the

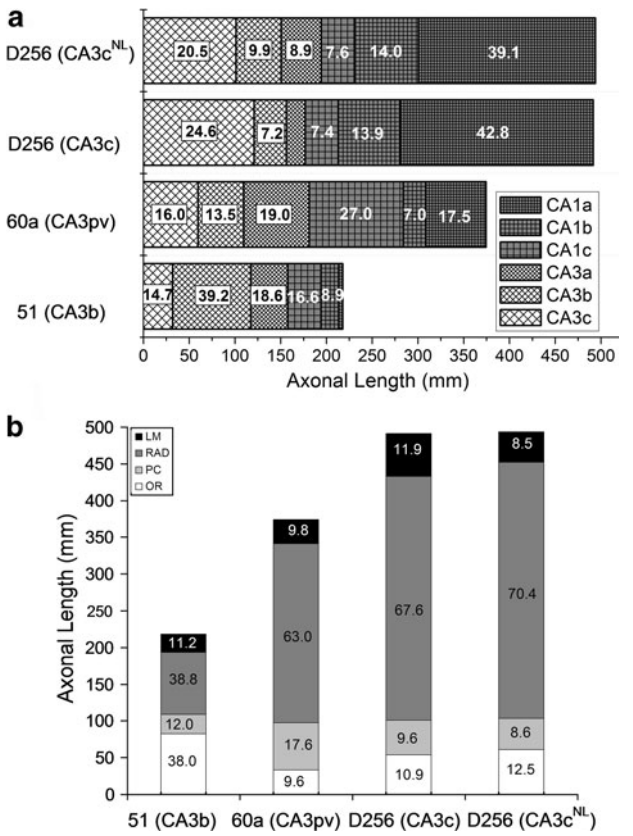

Fig. 5 Axonal length distributions across hippocampal sub-regions and layers. **a** Axonal collaterals for the four reconstructed neurons within each of six CA sub-regions (CA3c, CA3b, CA3a, CA1c, CA1b, and CA1a). *Bar lengths* are proportional to absolute measures, while the numerical labels in the *bars* indicate percentages within every neuron. **b** Axonal collaterals for the four reconstructed neurons within each of four individual layers (*OR* oriens, *PC* pyramidal cell, *RAD* radiatum, and *LM* lacunosum-moleculare). *Bar heights* are proportional to absolute measures, while the numerical labels in the *bars* indicate percentages within every neuron

CA3b and CA3c cells, more than half of the CA3 axonal collaterals recur within the somatic sub-region (Fig. 5a). In contrast, the CA3pv axons are more evenly spread in CA3, with only a modest preference for CA3a. Contrasting patterns are observed in the CA1 sub-regions, where two thirds of the axon from the CA3b neuron are located in CA1c, while two thirds of the axon from the CA3c neuron are located in CA1a. Once again the axon of the CA3pv neuron has features in common with both of the other cells, with a more balanced presence in CA1a and CA1c, but almost disregarding CA1b.

Consistent differences also emerge in the axonal distributions of the three pyramidal cells across layers. The CA3b neuron axons extend evenly between the superficial layers (strata oriens and pyramidale) and the deeper layers (strata radiatum and lacunosum-moleculare). In stark contrast, the axonal projection of the CA3c neuron is four times more prominent in deep than superficial layers

(Fig. 5b). As a reoccurring theme, the deep/superficial ratio is intermediate for the CA3pv neuron. Similar to the observation regarding the sub-regional patterns, these relative proportions reflect opposing absolute distributions. The total axonal length in the superficial layers is nearly the same for the three CA3 pyramidal cells (just above 100 mm), whilst the axonal presence of the CA3c neuron in the deep CA layers is more than three times that of the CA3b cell. Also as in the other analyses, both absolute and relative axonal values appear to be robust between the CA3c and $CA3^{NL}$ reconstructions both across layers and sub-regions (Fig. 5).

The approximately 10% of axonal length found in the pyramidal layer may appear surprising since these fibers do not form synapses on somata. A possible explanation for this finding is that digital reconstructions do not differentiate explicitly main axons from axon collaterals with boutons. We measured the mean axonal diameter in the pyramidal versus non-pyramidal layer, and we found no differences in any of the cells. Thus, the portions of the axons in the pyramidal cell layer are not thicker than the average branches. Another possibility is that axons in the pyramidal layer contact dendrites on the basal arbor of superficial neurons and apical arbors of deeper neurons.

Unique absolute and relative axonal distributions in specific CA3/CA1 circuit parcels

A more detailed view of the spatial distribution of the axonal arborization from each individual neuron is provided by a comparative examination of the length invading every layer and sub-region. This analysis effectively yields a map of the potential output of these CA3 pyramidal cells on the transverse "lamella" that captures much of Cornu Ammonis' poly-synaptic circuit. The three pyramidal cells are largely non-overlapping along the longitudinal axis of the hippocampus, rendering moot a direct comparison of their axonal distributions as a function of septo-temporal location. For each of the neurons, we first examined the relative sub-regional and layer composition of axonal length from the two portions of the arbor located septally and temporally relative to the soma. Having found only negligible differences (Figs. 2, 4), we report axonal length data summed across the longitudinal direction.

The absolute and relative distributions of axonal length by sub-region and layer are quantitatively represented by a pie chart for each of the neurons (Fig. 6). The total surface area of each chart is scaled relative to the total length of the corresponding neuronal arborizations, namely CA3b (top), CA3pv (middle), and CA3c (bottom). Within each pie

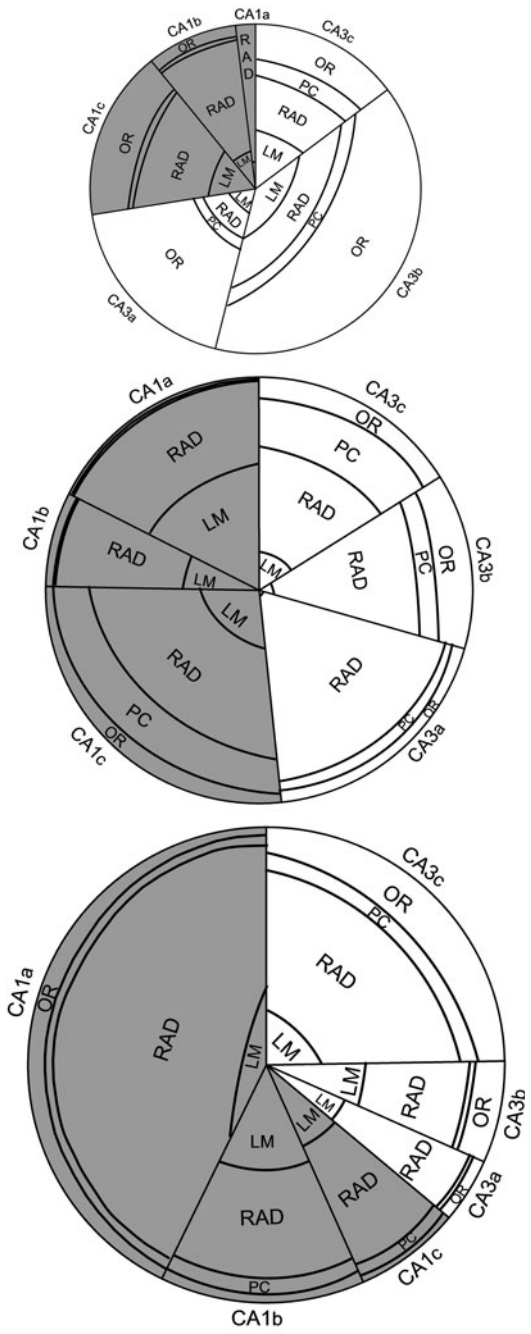

Fig. 6 Absolute and relative axonal length distributions within individual sub-regional layers. For each of the three neurons (CA3b *top*; CA3pv *middle*; CA3c *bottom*), the size of the *pie charts* is scaled according to total axonal length. The surface area of each pie slice is proportional to the axonal distributions in the respective three CA3 (*white*) and three CA1 (*gray*) sub-regions, and further divided based on the arbor length in each cytoarchitectonic layer (OR, PC, RAD and LM). These *pie charts* were generated by measuring sector surface areas with ImageJ (v.1.38, http://rsb.info.nih.gov/ij), and marking the appropriate slice boundary positions with Paint Shop Pro (v.8.0, http://corel.com)

chart, every slice has a surface area proportional to the axonal length in each of the three CA3 (white background) and three CA1 (gray background) sub-regions. All slices are further divided into four sectors with surface areas sized according to the represented cytoarchitectonic layers (from outermost to innermost: strata oriens, pyramidale, radiatum, and lacunosum-moleculare). Therefore, the ensemble view of the pie charts enables a relative assessment of the axonal composition among neurons, sub-regions, and layers. At the same time, the surface area of each of the slice sectors (and any of their combinations) constitutes a measure of the actual axonal length of the given cell in the corresponding hippocampal sub-region and layer, thus allowing absolute comparisons.

The axonal distributions among sub-regional layers follow the same general trends reported separately for the sub-regional compositions summed across layers and the layer compositions summed across sub-regions reported in Fig. 5. However, this more detailed analysis additionally reveals specific differences, which are most extreme between the CA3b and the CA3c cells. In the CA3b neuron, the oriens layer in CA3b alone accounts for nearly one-fifth (18%) of the entire axonal extent, compared, e.g., with a meager 2% in the radiatum layer of CA1a. In contrast, almost one-third of the whole axon of the CA3c neuron (32%) is found in the CA1a radiatum layer, as opposed to a negligible presence (<2%) in the CA3b oriens layer. Interestingly, the CA3b cell extends more oriens than radiatum axonal length in CA3, but more radiatum than oriens in CA1.

The differences between the CA3c and CA3b cells are somewhat blended in the CA3pv neuron, where stratum radiatum has a uniform axonal majority in all six CA sub-regions. Interesting trends are also shared among all three reconstructed neurons. In all cases, for example, the axonal length ratio between oriens and radiatum is greater in CA3 than in CA1 and, within CA1, increases moving transversally from the subicular end toward CA3 (CA1a–CA1c). In other words, there is more axon in radiatum than in oriens in both CA1 and CA3, but the proportion of the total that is in oriens is greater in CA1 and increases from the subiculum end of CA1 to the CA2 border.

The substantial differences in total axonal length among the three neurons yield a different perspective when comparing axonal distributions throughout the sub-regional layers in absolute, rather than relative, terms. For instance, the absolute axonal length of the CA3b neuron invading the oriens layer of area CA3b (39.3 mm) is very similar to the amount of CA3c axon invading the radiatum layer of area CA1b (41.3 mm), even if they constitute very different fractions of their respective arbors (18 vs. 8.4%, respectively). In contrast, the same 8.4% fraction of the CA3b neuron occupying the oriens layer of area CA3a only amounts to a length of 18.4 mm. Likewise, the axonal length of the CA3b neuron found in the radiatum layer of area CA3b (26.2 mm) closely matches the value for the CA3c neuron in the radiatum layer of area CA1c (25.5 mm), while their relative proportions are more than twofold off (12 vs. 5.2%). A similar 5.1% proportion of the CA3b neuron invading the radiatum layer of area CA3c corresponds to an absolute length of just 11 mm.

In some cases, the absolute size differences among neurons accentuate, rather than compensate, the non-uniform relative distributions across sub-regional layers. For example, in terms of absolute length, stratum radiatum of area CA1a receives 36 times more axon from the CA3c neuron than from the CA3b neuron (156 vs. 4.3 mm). These observations were qualitatively confirmed post-hoc by direct microscopic inspection of the slices. For example, inspection of the CA3b neuron slide revealed very sparse axonal presence in the radiatum layer of area CA1a, while the same region of interest displayed dense axonal labeling in the CA3c neuron slide.

Discussion

Axonal morphology sculpts network connectivity (Stepanyants and Chklovskii 2005; Stepanyants et al. 2008) and intrinsic neuronal processing (Manor et al. 1991; Debanne 2004). Thus, its quantitative characterization is crucial to understand structure–function relationship in the brain. Modern computer-interfaced microscopes and commercial software (e.g. NeuroLucida) allow the direct reconstruction of imaged neuronal arbors into digital format (Ascoli 2006). In practice, however, the ergonomics of the human–equipment interaction typically restrict this possibility to neurites of limited extent, such as dendritic trees or local axons. Larger projections, like axons of principal cells in the mammalian cortex, are more commonly only traced "pencil-on-paper" by simple Camera Lucida technique. Unfortunately, the resulting analog drawings are less conducive to quantitative analysis.

In this work, we extended a semi-automated approach for digitally reconstructing neuronal arbors all the way back to the initial step of basic Camera Lucida, allowing the first quantitative analysis of multiple CA3 pyramidal cell axons intracellularly labeled in vivo. Evaluating intrinsic cell-to-cell variability beyond single neuron samples from each of distinct area (CA3c, CA3b, and CA3pv) will require even greater automation (Ascoli 2008). At the same time, full axonal arbors are dozens of times larger than typical dendritic trees, making these reconstructions remarkably data-rich. Previous studies proved even individual axon reconstructions to be deeply informative (e.g. Sik et al. 1993; Tamamaki et al. 1988).

Here, we used the only one of these previously acquired data files that is independently available in digital format (Wittner et al. 2007) to validate our novel semi-automated digitization system by reconstructing the same cell from the same slides. All morphometric measures employed in this report showed excellent consistency between these two data files.

To appreciate the massiveness of these axonal tracings it is useful to compare these morphologies with other digital reconstructions available from NeuroMorpho.Org, the largest available collection of neuronal tracings (Ascoli et al. 2007), and relevant hippocampal literature. A dentate gyrus granule cell filled in vivo has total axonal lengths of approximately 9 mm (Scorcioni and Ascoli 2005), which is only ~3 times that of the dendritic arborization for the same cell type (e.g. Claiborne et al. 1990). Hippocampal interneurons from CA3b strata radiatum and lacunosum-moleculare have typical axonal and dendritic lengths of ~20 and ~3 mm, respectively (Ascoli et al. 2009), but their completeness cannot be established conclusively since these were injected in slices. One of the interneuron described from the dentate gyrus had very extensive axonal arbor, potentially comparable to that of pyramidal cells (Sik et al. 1997). Although not fully reconstructed, long-range interneurons also have very dense axons (Sik et al. 1994). Because of their substantially larger axon caliber (Jinno et al. 2007) the total axonal volume of these long-range interneurons can be several times larger than that of pyramidal cells.

At the same time, other principal neurons from the mammalian cerebral cortex in NeuroMorpho.Org have axonal length of the same order of magnitude as the values reported here, such as a pyramidal cell from the visual cortex of the cat at ~110 mm even if incomplete (Hirsch et al. 2002), a spiny stellate cell from the entorhinal cortex of the rat at ~160 mm without including full local collaterals (Tamamaki and Nojyo 1995), and a CA2 pyramidal cell from the rat hippocampus at ~430 mm (Tamamaki et al. 1988). Except for the cat visual cortex example, all these other principal cell axonal reconstructions were obtained with the previous version of the semi-automated reconstruction technique employed here (Scorcioni and Ascoli 2005). In sharp contrast, axons traced from cells intracellularly filled in the slice have much more contained axonal length most probably due to axotomy. For example, pyramidal cells from monkey prefrontal cortex have total axonal length of ~35 mm (Gonzalez-Burgos et al. 2004). Therefore, in terms of data density, the three CA3 pyramidal cell axonal reconstructions described here and publicly distributed at NeuroMorpho.Org contribute great potential for subsequent analysis and modeling.

The ipsilateral axonal projections of CA3 pyramidal neurons generate two crucial associational pathways in the neurobiology of learning and memory: the recurrent collaterals within area CA3 and the Schaffer collaterals into area CA1. Previous studies (Ishizuka et al. 1990; Li et al. 1994) indicated that the relative balance of these two systems depends on the longitudinal and transverse location of the presynaptic cell, as well as the targeted sub-regions (CA3/CA1a,b,c) and layers (oriens/radiatum). By embedding three digitally reconstructed axons within a 3D template of the rat hippocampus, our approach quantified specific patterns of axonal collaterals throughout every cytoarchitectonic location along the septo-temporal axis.

In dorsal hippocampus, dramatic quantitative differences were measured between CA3c and CA3b pyramidal cells. The CA3c neuron projected twice as much axon to CA1 as to CA3, and, within CA1, twice as much in CA1a (distally) than in CA1b and CA1c combined. Throughout these regions, this axonal arbor overwhelmingly preferred stratum radiatum to oriens by a 6:1 ratio. In contrast, the CA3b neuron projected thrice as much axon to CA3 than to CA1, and, within CA3, 50% more to CA3b (locally) than to CA3a and CA3c combined. Within CA1, this neuron extended 50% more length in CA1c (proximally) than in CA1a and CA1b combined. While within CA3b the recurrent collateral preferred stratum oriens to radiatum by 50% margin, the trend was reversed in the Schaffer projections to CA1, where radiatum trumped oriens 3:1.

Such diametrical opposition suggests a possible sub-regional and cytoarchitectonic specialization for the dual organization of CA3 axons into recurrent and Schaffer collaterals, as also reflected by physiological studies (Csicsvari et al. 2000, 2003). Distal projections to CA1 predominate in CA3c and preferentially target the radiatum layer. Local arbors predominate in CA3b and preferentially target the oriens layer. This putative division could in turn hint to an alteration of the classic view of the hippocampal synaptic circuit. Rather than region uniform receiving entorhinal input (directly and through the dentate gyrus) and transmitting output to CA1, area CA3 might be serially composed of a first station (CA3b) suitable to receive and locally distribute input within CA3, followed by a second station (CA3c) mainly dedicated to propagate the output downstream to CA1. This alternative view is also supported by prominent dendritic branching (>15% of total dendritic length) of CA3b pyramidal cells in stratum lacunosum-moleculare (the layer invaded by the entorhinal perforant pathway) compared with almost negligible dendritic presence (<3% of total dendritic length) of CA3c neurons in this layer (Ishizuka et al. 1995).

The opposite trends observed in CA3c and CA3b neurons from the dorsal hippocampus are somewhat blended in the pyramidal cells reconstructed from the posterior/ventral area, with axonal collaterals more uniformly distributed throughout all sub-regions. The substantial differences in

total arbor length among the reconstructed neurons combine with their relative differences in sub-region and layer distributions, resulting in relative constant absolute values of axonal extent, e.g. in the combined oriens and pyramidal layers (very close to 100 mm for all three cells) or within sub-regions CA3a,b,c together (~170 mm for all three cells). Thus, pyramidal cell output might be specifically differentiated for selective targets (CA1 and radiatum), yet relatively stable for others.

Recent studies reported CA3 back-projections to the dentate gyrus (Scharfman 2007), especially towards the temporal pole (Witter 2007). Also at least one neuron described in the ventral hippocampus (cell r32 in Li et al. 1994) extensively collateralized in the dentate molecular layer. For each of our three neurons, the axonal length within the hilus fell within the margin of measurement error (2–2.5%) and was neglected. Another open question not tackled by the present study regards the relative extent of the commissural projection to the controlateral hippocampus.

Functionally, the CA3 region is recognized to play important roles in memory encoding and retrieval (Treves and Rolls 1994; Treves 2004; Kunec et al. 2005). In most physiological, behavioral, and computational studies, CA3 is considered a single functional region. Recently, however, lesion studies in the rat showed dissociation between CA3 sub-regions (Hunsaker et al. 2008). Specifically, CA3c lesions yielded greater spatial deficits than lesions in sub-regions CA3a and CA3b. These sub-regions are also differentially involved in initiating and transferring population patterns (Csicsvari et al. 2000). Such functional specialization of individual CA3 sub-regions (Kesner 2007) is consistent with the differential axonal collateral patterns of CA3c and CA3b pyramidal cells demonstrated here.

Lesion studies also revealed dorso-ventral functional differentiation (Bannerman et al. 1999; Hock and Bunsey 1998; Hunsaker and Kesner 2008), whereas dorsal, but not ventral, rat hippocampus appears involved in spatial behavior, as also supported by physiological observations (Royer et al. 2010). Differing circuit organizations might underlie the functional dissociation of dorsal and ventral hippocampus (Moser and Moser 1998). Among the neurons we reconstructed, the posterior/ventral pyramidal cell displayed an axonal distribution pattern intermediate between those of CA3c and CA3b neurons in dorsal hippocampus. This might indicate a less distinct sub-regional differentiation in ventral than in dorsal hippocampus, consistent as well with the relatively more uniform axonal distribution of the CA3pv cell among individual cytoarchitectonic layers throughout the six CA3/CA1 areas.

Axonal reconstructions can be utilized to estimate potential synaptic connectivity patterns based on geometrical overlaps with dendritic arbors (Stepanyants et al. 2002; Kalisman et al. 2003). While thousands of digital dendritic reconstructions are readily available in the public domain (Ascoli et al. 2007), no axons have been fully traced for most known neuron classes. The free distribution of the digital morphologies described here through the NeuroMorpho.Org database should thus constitute a useful addition to shared neuroscience resources. Axonal territory provides a map of necessary, but not sufficient conditions to characterize synaptic connectivity, as individual synapses might abide specific, localized, and compartmentalized criteria (Shepherd and Harris 1998). In the hippocampus, however, axo-dendritic overlap predicts actual contacts in at least some neuron types (Stepanyants et al. 2004). In the heydays of connectomics (Kennedy 2010), the key information about networks is quantitative neuronal connectivity in vivo. Complete axonal arbors of single neurons are still unsolvable with any of the ongoing connectomics approaches due to limits of resolution (non-invasive imaging), sampling (fluorescent genetic labeling) or field-of-view (electron microscopy). Although time-consuming, intracellular labeling is critical to elucidate connections between neuron types.

Axonal signal propagation also depends on the geometry of its arbor. The intrinsic axonal length properties of CA3 pyramidal cells could affect action potential conduction velocity and even branch point failure in these complex 3D arbors. These effects might influence spike timing and delays, therefore imposing noteworthy computational constraints on temporal coding (Carr and Konishi 1990; McAlpine and Grothe 2003). Although we are still at the beginning of the path towards understanding how the functions of the nervous system emerge from the structure and activity of its circuit, this study represents a step forward in elucidating the morphological organization of one of the most plastic networks in the adult mammalian brain.

Acknowledgments We are indebted to Todd Gillette and Maryam Halavi for their valuable feedback on an earlier version of this manuscript, to Aruna Muthulu for scanning and aligning the tracings, and to Lucia Wittner for sharing reconstruction CA3c^{NL} on NeuroMorpho.Org. Grant sponsor: National Institute of Health Grant numbers: NS39600 & NS058816 to GAA, and NS34994 & MH54671 to GB.

References

Ascoli GA (2006) Mobilizing the base of neuroscience data: the case of neuronal morphologies. Nat Rev Neurosci 7:318–324

Ascoli GA (2008) Neuroinformatics grand challenges. Neuroinformatics 6:1–3

Ascoli GA, Donohue DE, Halavi M (2007) NeuroMorpho.Org: a central resource for neuronal morphologies. J Neurosci 27:9247–9251

Ascoli GA, Brown KM, Calixto E, Card JP, Galvan EJ, Perez-Rosello T, Barrionuevo G (2009) Quantitative morphometry of electrophysiologically identified CA3b interneurons reveals robust local geometry and distinct cell classes. J Comp Neurol 515:677–695

Bannerman DM, Yee BK, Good MA, Heupel MJ, Iversen SD, Rawlins JN (1999) Double dissociation of function within the hippocampus: a comparison of dorsal, ventral, and complete hippocampal cytotoxic lesions. Behav Neurosci 113:1170–1188

Buzsaki G (1986) Hippocampal sharp waves: their origin and significance. Brain Res 398:242–252

Carr CE, Konishi M (1990) A circuit for detection of interaural time differences in the brain stem of the barn owl. J Neurosci 10:3227–3246

Claiborne BJ, Amaral DG, Cowan WM (1990) Quantitative, three-dimensional analysis of granule cell dendrites in the rat dentate gyrus. J Comp Neurol 302:206–219

Csicsvari J, Hirase H, Mamiya A, Buzsaki G (2000) Ensemble patterns of hippocampal CA3-CA1 neurons during sharp wave-associated population events. Neuron 28:585–594

Csicsvari J, Jamieson B, Wise KD, Buzsaki G (2003) Mechanisms of gamma oscillations in the hippocampus of the behaving rat. Neuron 37:311–322

Debanne D (2004) Information processing in the axon. Nat Rev Neurosci 5:304–316

Gonzalez-Burgos G, Krimer LS, Urban NN, Barrionuevo G, Lewis DA (2004) Synaptic efficacy during repetitive activation of excitatory inputs in primate dorsolateral prefrontal cortex. Cereb Cortex 14:530–542

Hirsch JA, Martinez LM, Alonso JM, Desai K, Pillai C, Pierre C (2002) Synaptic physiology of the flow of information in the cat's visual cortex in vivo. J Physiol 540:335–350

Hock BJ Jr, Bunsey MD (1998) Differential effects of dorsal and ventral hippocampal lesions. J Neurosci 18:7027–7032

Hunsaker MR, Kesner RP (2008) Dissociations across the dorsal-ventral axis of CA3 and CA1 for encoding and retrieval of contextual and auditory-cued fear. Neurobiol Learn Mem 89:61–69

Hunsaker MR, Rosenberg JS, Kesner RP (2008) The role of the dentate gyrus, CA3a, b, and CA3c for detecting spatial and environmental novelty. Hippocampus 18:1064–1073

Ishizuka N, Weber J, Amaral DG (1990) Organization of intrahippocampal projections originating from CA3 pyramidal cells in the rat. J Comp Neurol 295:580–623

Ishizuka N, Cowan WM, Amaral DG (1995) A quantitative analysis of the dendritic organization of pyramidal cells in the rat hippocampus. J Comp Neurol 362:17–45

Jinno S, Klausberger T, Marton LF, Dalezios Y, Roberts JD, Fuentealba P, Bushong EA, Henze D, Buzsaki G, Somogyi P (2007) Neuronal diversity in GABAergic long-range projections from the hippocampus. J Neurosci 27:8790–8804

Kalisman N, Silberberg G, Markram H (2003) Deriving physical connectivity from neuronal morphology. Biol Cybern 88:210–218

Kennedy DN (2010) Making connections in the connectome era. Neuroinformatics 8:61–62

Kesner RP (2007) Behavioral functions of the CA3 subregion of the hippocampus. Learn Mem 14:771–781

Kunec S, Hasselmo ME, Kopell N (2005) Encoding and retrieval in the CA3 region of the hippocampus: a model of theta-phase separation. J Neurophysiol 94:70–82

Li XG, Somogyi P, Ylinen A, Buzsaki G (1994) The hippocampal CA3 network: an in vivo intracellular labeling study. J Comp Neurol 339:181–208

Lorente de Nó R (1934) Studies on the structure of the cerebral cortex II. Continuation of the study of the ammonic system. J Psychol Neurol 46:113–117

Manor Y, Koch C, Segev I (1991) Effect of geometrical irregularities on propagation delay in axonal trees. Biophys J 60:1424–1437

McAlpine D, Grothe B (2003) Sound localization and delay lines–do mammals fit the model? Trends Neurosci 26:347–350

Moser MB, Moser EI (1998) Functional differentiation in the hippocampus. Hippocampus 8:608–619

Pyapali GK, Sik A, Penttonen M, Buzsaki G, Turner DA (1998) Dendritic properties of hippocampal CA1 pyramidal neurons in the rat: intracellular staining in vivo and in vitro. J Comp Neurol 391:335–352

Ramón y Cajal S (1911) Histologie du Système Nerveux. Maloine, Paris

Rolls ET (2007) An attractor network in the hippocampus: theory and neurophysiology. Learn Mem 14:714–731

Ropireddy D, Bachus S, Scorcioni R, Ascoli GA (2008) Computational neuroanatomy of the rat hippocampus: implications and application to epilepsy. In: Soltesz I, Staley K (eds) Computational neuroscience in epilepsy. Elsevier, San Diego, pp 71–85

Royer S, Sirota A, Patel J, Buzsaki G (2010) Distinct representations and theta dynamics in dorsal and ventral hippocampus. J Neurosci 30:1777–1787

Scharfman HE (2007) The CA3 "backprojection" to the dentate gyrus. Prog Brain Res 163:627–637

Scorcioni R, Ascoli GA (2005) Algorithmic reconstruction of complete axonal arborizations in rat hippocampal neurons. Neurocomputing 65–66:15–22

Scorcioni R, Polavaram S, Ascoli GA (2008) L-Measure: a web-accessible tool for the analysis, comparison and search of digital reconstructions of neuronal morphologies. Nat Protoc 3:866–876

Shepherd GM, Harris KM (1998) Three-dimensional structure and composition of CA3 → CA1 axons in rat hippocampal slices: implications for presynaptic connectivity and compartmentalization. J Neurosci 18:8300–8310

Sik A, Tamamaki N, Freund TF (1993) Complete axon arborization of a single CA3 pyramidal cell in the rat hippocampus, and its relationship with postsynaptic parvalbumin-containing interneurons. Eur J Neurosci 5:1719–1728

Sik A, Ylinen A, Penttonen M, Buzsaki G (1994) Inhibitory CA1-CA3-hilar region feedback in the hippocampus. Science 265:1722–1724

Sik A, Penttonen M, Buzsaki G (1997) Interneurons in the hippocampal dentate gyrus: an in vivo intracellular study. Eur J Neurosci 9:573–588

Stepanyants A, Chklovskii DB (2005) Neurogeometry and potential synaptic connectivity. Trends Neurosci 28:387–394

Stepanyants A, Hof PR, Chklovskii DB (2002) Geometry and structural plasticity of synaptic connectivity. Neuron 34:275–288

Stepanyants A, Tamas G, Chklovskii DB (2004) Class-specific features of neuronal wiring. Neuron 43:251–259

Stepanyants A, Hirsch JA, Martinez LM, Kisvarday ZF, Ferecsko AS, Chklovskii DB (2008) Local potential connectivity in cat primary visual cortex. Cereb Cortex 18:13–28

Tamamaki N, Nojyo Y (1995) Preservation of topography in the connections between the subiculum, field CA1, and the entorhinal cortex in rats. J Comp Neurol 353:379–390

Tamamaki N, Abe K, Nojyo Y (1988) Three-dimensional analysis of the whole axonal arbors originating from single CA2 pyramidal neurons in the rat hippocampus with the aid of a computer graphic technique. Brain Res 452:255–272

Treves A (2004) Computational constraints between retrieving the past and predicting the future, and the CA3-CA1 differentiation. Hippocampus 14:539–556

Treves A, Rolls ET (1994) Computational analysis of the role of the hippocampus in memory. Hippocampus 4:374–391

Turner DA, Li XG, Pyapali GK, Ylinen A, Buzsaki G (1995) Morphometric and electrical properties of reconstructed hippocampal CA3 neurons recorded in vivo. J Comp Neurol 356:580–594

Witter MP (2007) Intrinsic and extrinsic wiring of CA3: indications for connectional heterogeneity. Learn Mem 14:705–713

Witter MP, Amaral DB (2004) Hippocampal formation. In: Paxinos G (ed) The rat nervous system. Elsevier, San Diego, pp 635–704

Wittner L, Henze DA, Zaborszky L, Buzsaki G (2007) Three-dimensional reconstruction of the axon arbor of a CA3 pyramidal cell recorded and filled in vivo. Brain Struct Funct 212:75–83

Wolf E, Birinyi A, Pomahazi S (1995) A fast 3-dimensional neuronal tree reconstruction system that uses cubic polynomials to estimate dendritic curvature. J Neurosci Methods 63:137–145